Turkish Journal of Electrical Engineering & Computer Sciences

http://journals.tubitak.gov.tr/elektrik/

Research Article

Turk J Elec Eng & Comp Sci
(2014) 22: 768 – 779

doi:10.3906/elk-1205-47

Retinal image analysis using multidirectional functors based on geodesic conversions

Saleh SHAHBEIG*
Department of Electrical Engineering, Najafabad Branch, Islamic Azad University, Isfahan, Iran

Received: 17.05.2012 • **Accepted:** 07.09.2012 • **Published Online:** 21.03.2014 • **Printed:** 18.04.2014

Abstract: A retinal image contains vital information. Extracting these features is the first and most important step in the analysis of retinal images for various applications of medical or human recognition. In this study, a morphological-based blood vessel extraction algorithm using adaptive-local analysis from colored retinal images is proposed. In this algorithm, by applying the appropriate morphology functors and local histogram stretching on the retinal images, the brightness of the images is considerably uniformed. Furthermore, curvelet transform (CT) is used to enhance the retinal images by highlighting the edges of the images in various scales and directions and by the adaptive and local improving of the CT coefficients. Since the blood vessels in retinal images are distributed in various directions, we use the morphology functors with multidirectional structure elements to extract the blood vessels from the retinal images. Geodesic conversion-based morphology functors are used to properly refine the appeared frills with a size smaller than those of the arterioles in the images. Finally, by locally applying the connected component analysis in the images and locally applying an adaptive filter on the connected components, all of the residual frills are refined from the images. The obtained results of the proposed algorithm show that the blood vessels are extracted from the background of the images with high accuracy, which in turn shows the high ability of the proposed algorithm in extracting the retinal blood vessels.

Key words: Blood vessel extraction, retinal image, curvelet transform, adaptive-local analysis, geodesic conversion-based morphology functors, multidirectional morphology functors

1. Introduction

One of the most important internal components in the eye is the retina, covering the entire posterior compartment, on which all of the optic receptors are distributed. Disorders of the retina resulting from special diseases are diagnosed by special images of the retina that are obtained using optic imaging called fundus photography. Blood vessels are important parts of retinal images, consisting of arteries and arterioles. Checking the obtained changes in retinal images in a special period can help the physician to diagnose disease. Applications for retinal images include diagnosing the progress of some cardiovascular diseases, diagnosing the region with no blood vessels (macula), using such images in helping automatic laser surgery on the eye, and using such images in biometric applications. On the other hand, extracting retinal blood vessels is done in some cases by a physician manually, which is difficult and time-consuming, and is accompanied by many mistakes due to much dependence on the physician's skill level. Hence, the exact extraction of the blood vessels from the retinal images necessitates using an algorithm and instruments that reduce the dependency on the functor and eliminate the error factors. Among the most common methods used to extract the blood vessels, tracking-based

*Correspondence: saleh_shahbeig@sel.iaun.ac.ir

[1], classifying-based [2], and window-based [3] methods can be referenced. Because of the variability of the light reflection coefficient in different parts of the retina layer, which are also due to the defects in imaging systems, there occurs very nonuniform illumination in the retinal images, which impairs modeling the blood vessels in window-based methods and tracking in tracking-based methods. Since all of the connected regions in the retinal images are classified by a low-level algorithm in classifying-based methods, the pixels related to the blood vessels cannot be classified carefully due to the intrinsic noise in the retinal images and oscillating changes in the image illumination. Hence, for the extraction of blood vessels with high accuracy, we need an effective algorithm.

In this paper, using appropriate morphology functors [4] and locally applying the histogram stretching, the illumination of an image is uniformed. Since the preprocessing phase plays an important role in the final extraction results, locally applying the morphology functors and histogram stretching on a retinal image will have a noticeable effect on improving the accuracy of the final edge image. Next, by locally applying an adaptive function [5] on the curvelet coefficients [6], along with amplifying the desired signal and enhancing the image contrast, amplifying of the noise is prevented. One of the advantages of the proposed algorithm is applying the histogram stretching locally and curvelet transform on the image to reduce the noise and improve the contrast. Therefore, the inadequacy of previous methods is resolved. Since the blood vessels are distributed in different directions, we use the morphology functors [7] with multidirectional structure elements to extract the blood vessels from retinal images. Applying the multidirectional structure elements in this study causes the blood vessels to be separated from the background with high accuracy. Finally, using geodesic conversion-based morphology functors, connected component analysis (CCA), and locally applying the adaptive filter on the connected components with a defined threshold [8], the frills in the image are removed and the extracted blood vessels are obtained.

The rest of the paper is organized as follows: In Section 2, the proposed algorithm is described. In Section 2.1, the preprocessing phase is introduced. In Section 2.2, the blood vessel extraction method is described. The frill deleting method is described in Section 2.3. In Section 3, the experimental results are presented and discussed. Conclusions are presented in Section 4.

2. Proposed retinal image blood vessel extraction algorithm

Figure 1 shows a summary of the proposed algorithm. First, the step of preprocessing is done on the images to extract the retinal blood vessels from the color images.

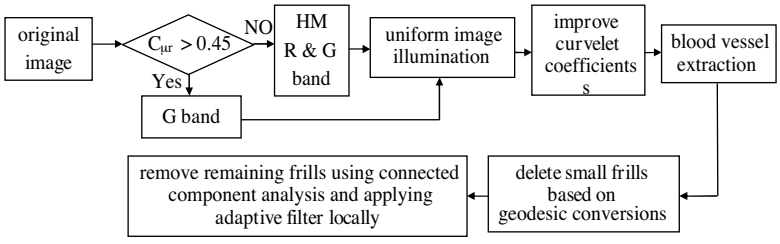

Figure 1. Summary of the proposed algorithm.

The images taken from retina are colored ones, so we can convert them into gray images with the best contrast. For this purpose, we decompose the original and color images into subbands of red, green, and blue, and then by defining the criterion $C_{\mu r}$, we select the best subband in terms of the dynamic range and signal rate [8]. Since the nonuniformity of the illumination in the retinal images generates frills in the final edge image,

it is necessary to uniform the image illumination. The BotHat morphology function [4] and local histogram stretching are then used to uniform the illumination of the images. The BotHat morphology function, with an appropriately sized structure element, produces an image with a uniformed background and highlighted blood vessels.

Locally applying the histogram stretching on the produced images increases the dynamic range of the gray levels of the image's components considerably and highlights the image data. Since enhancing the edges of the image increases the contrast, using the multiscale and multidirectional curvelet transform [6], the edges of image are enhanced. Selecting the adaptive nonlinear function [5] and locally applying it on the curvelet coefficients of the retinal images enhances the contrast of the retinal images. To start the process of extracting the retinal blood vessels, we use the improved TopHat function [7] with multidirectional structure elements. There occur some frills in the extracted blood vessel image (edge image) in addition to the extracted blood vessels because of the intrinsic noise in the retinal images. Applying the morphology functors based on geodesic conversions to delete the frills smaller than arterioles and then locally applying the CCA and adaptive filter to delete the rest of frills are proposed in this study. Finally, the image of the blood vessels is extracted from the retinal image.

3. Preprocessing

3.1. Selecting the proper subband of image

The subband G (green) from the colored retinal images has the best contrast by experience, but sometimes it has a low contrast. Hence, in this study, to get the best gray images from colored retinal images, the criterion $C_{\mu r}$ is defined in the following equation [8]:

$$C\mu r = \sum_{j=0}^{\mu r} (p_r(r_j)), \tag{1}$$

where μ_r is the mean of the gray levels in the image of subband R (red) and $C_{\mu r}$ is the sum of the probability density function ($p_r(.)$) of the gray level from $r_j = 0$ to $r_j = \mu_r$, related to subband G. For example, if $C_{\mu r} > 0.45$, it means that the illumination of subband G is proper, and we use only it in the rest of the process; otherwise, we increase the dynamic range of the gray level of subband G by histogram matching and with the aid of subband R.

3.1.1. Curvelet transform

The curvelet transform [6] is considered as a new generation multiscale transform, which results in a set of coefficients in various directions and scales by applying a specific wavelet in different directions and scales on the image. Each of these sets of coefficients, located in a polar wedge in the frequency domain, indicates data from the image in that scale and direction. Curvelet transform in this section works throughout in 2 dimensions, $\Re^2$, with spatial-domain variable x, frequency-domain variable ω, and r and θ, which are polar coordinates in the frequency domain.

At first, a pair of windows, W(r) and V(t), must be defined, which are called the 'radial window' and 'angular window', respectively. These are smooth, nonnegative, and real-valued. The radial window takes positive real arguments and is supported on $r \in (1/2\ ,2)$, and the angular window takes real arguments and is supported on t $\in [-1,1]$.

Now, for each scale 'j', where $j \geq j_0$, the frequency window U_j is defined in the Fourier domain by Eq. (2):

$$U_j(r,\theta) = 2^{-3j/4} W(2^{-j}r) V(\frac{2\lfloor j/2 \rfloor \theta}{2\pi}), \tag{2}$$

where $\lfloor j/2 \rfloor$ is the integer part of $j/2$. Thus, U_j covers an area that is a polar 'wedge', where this range is determined by the radial and angular windows (W and V).

The width of the range in each direction will depend on the scale. We work with the symmetrized version of Eq. (2), namely $U_j(r,\theta) + U_j(r,\theta+\pi)$, to obtain the real-valued curvelets.

The waveform $\phi_j(x)$ by means of its Fourier transform is defined as $\widehat{\phi}_j(x) = U_j(\omega)$. Here, ϕ_j can be considered as a 'mother' curvelet. Thus, all of the curvelets at scale 2^{-j} will get the rotations and translations of ϕ_j. Now, we introduce:

- the equally spaced sequence of rotation angles $\theta_l = 2\pi 2^{-\lfloor j/2 \rfloor} l$, with $l = 0, 1, \ldots$, such that $0 \leq \theta_l < 2\pi$,
- and the sequence of translation parameters $k = (k_1, k_2) \in \mathrm{Z}^2$.

With these notations, the curvelets (as a function of $\mathrm{x} = (\mathrm{x}_1, \mathrm{x}_2)$) at scale 2^{-j}, with orientation θ_l and position $x_k^{(j,l)} = R_{\theta_l}^{-1}(k_1.2^{-j}, k_2.2^{-j/2})$, are defined by the following equation:

$$\phi_{j,l,k}(x) = \phi_j(R_{\theta_l}(x - x_k^{(j,l)})), \tag{3}$$

where R_{θ_l} is the rotation by θ_l radians and is defined in the following equation:

$$R_{\theta_l} = \begin{pmatrix} Cos\theta_l & Sin\theta_l \\ -Sin\theta_l & Cos\theta_l \end{pmatrix}. \tag{4}$$

A curvelet coefficient is then simply the inner product between an element $f \in L^2(\Re^2)$ and a curvelet $\phi_{j,l,k}$.

$$C(j,l,k) = \langle f, \phi_{j,l,k} \rangle \tag{5}$$

Since digital curvelet transforms operate in the frequency domain, it will prove useful to apply Plancherel's theorem and express this inner product as the integral over the frequency plane.

$$C(j,l,k) = \frac{1}{(2\pi)^2} \int f(\omega) U_j(R_{\theta l}\omega) e^{i\left\langle x_k^{(j,l)},\, \omega \right\rangle} d\omega \tag{6}$$

Here, f is the Fourier transform of the signal and U_j is the frequency window applied in the frequency domain.

Hence, $C(j,l,k)$ is achieved in the scale j, direction l, with the transition parameter k. Figure 2 shows the tiling of the curvelet in the frequency plane. The curvelet in the frequency domain covers approximate parabolic wedges. The shaded area shows one of the typical wedges.

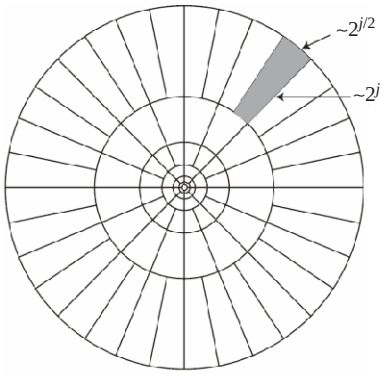

Figure 2. Curvelet tiling of the frequency plane.

Further details and equations relating to the curvelet transform were given in [6] as a new generation of multiscale transforms.

3.1.2. Adaptive function locally applied on the curvelet coefficients of the image

The parameters for the adaptive function [5] are defined in Eq. (3), based on some statistical characteristics of the curvelet coefficients of the input image, which result in the curvelet coefficients being improved more effectively. Because the defining of the parameters of the adaptive function is based on the statistical characteristics of the curvelet coefficients of the input image, if we apply the following adaptive function on the uniformed image coefficients, the function acts adaptively and adapts itself to each input image and based on the statistical characteristics of the curvelet coefficients of that image. In addition to amplifying the desired signal, it prevents the noise from being increased simultaneously, so the inadequacy of the previous methods is resolved.

$$y(x) = \begin{cases} k_1(\frac{m}{c})^p & \text{if} \quad |x| < ac \\ k_2(\frac{m}{|x|})^p & \text{if} \quad ac \le |x| < m \\ k_3 & \text{if} \quad m \le |x| \end{cases} \tag{7}$$

Here, p is the degree of the function nonlinearity; k_1, k_2, and k_3 are the coefficients of such a function; and m is defined as:

$$m = k(M_{ij} - \sigma), \tag{8}$$

where M_{ij} is the greatest coefficient in a specific scale and direction indicating that the coefficients are improved in every band according to their maximum value. $C = \sigma$ is the standard deviation of the estimated noise from image [9], which prevents noise from being increased while amplifying the desired signal simultaneously. Two parameters, M_{ij} and c, lead the above function to act adaptively and to adapt itself to different input images. The above function increases the small coefficients more than the bigger ones. This function is applied on the coefficients locally, where M_{ij} is calculated in any specific scale and direction and then the aforesaid function is applied on the coefficients of this polar wedge (frequency band with specific scale and direction); this, in turn, influences the image more.

3.2. Blood vessel extraction by morphology functors and multidirectional structure elements

Many morphology functions are applied for extracting blood vessels; for example, the TopHat function is one of them, but the problem with this function is that the pixels in the resulting image from applying the opening

function have gray-level values equal to or less than corresponding pixels in the original image. In this paper, the improved TopHat function [7] was used to extract blood vessels from the background of retinal images. The improved TopHat function [7] is defined as:

$$TopHat = I - \min((I \bullet S_c) \circ S_o; I). \tag{9}$$

In the output of the improved TopHat function, an image is produced that is equal to the original one, except for the edges, so the sensitivity to the noise is resolved. S_o and S_c are the structure elements applied to opening and closing morphology functions. $\circ$ and $\bullet$ are the opening and closing markers. Since the blood vessels and arterioles are distributed in different directions in the retinal image, using a simple structure element is not effective, and so in this paper, we apply the multidirectional structure elements in the improved TopHat function [7]. For instance, Figure 3 shows some of the substructure elements with dimensions of 7 $\times$ 7 and an angular accuracy of 15°.

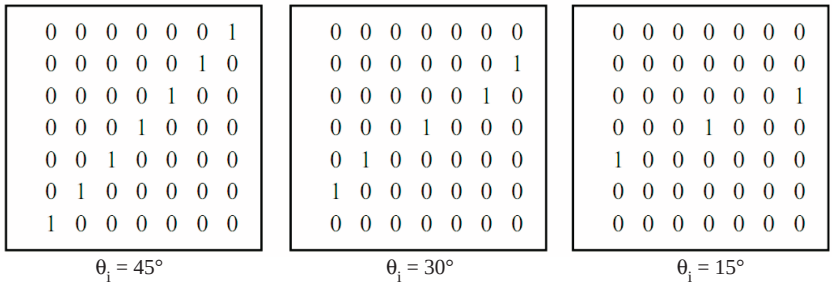

Figure 3. Substructure elements with dimensions of 7 $\times$ 7.

Each of the structure elements with a specific direction is able to extract a specific direction of the data in the blood vessel image. The final edge image, which is the extracted blood vessel image, is obtained through a linear combination of such subimages of the edge. It can be written as in Eq. (10):

$$F(I) = \sum_{i=0}^{M-1} \omega_i F(I)_i. \tag{10}$$

On the other hand, we define the weights ω_i so that each resulting subimage of the edge can influence the final edge image, depending on the existing data therein.

3.3. Deleting frills

3.3.1. Applying morphology functors based on geodesic conversions

If we consider a second image in addition to the main image and it is imposed in any step of the morphology dilation or erosion, where the resulting image remains bigger or smaller than the second image, the fundamentals of the morphology functors based on geodesic conversions are formed [10]. If the functors are repeated successively until the stability time, they introduce robust algorithms. Applying the opening functor based on geodesic conversions [10] with multidirectional structure elements, as introduced in the previous section, deletes some of the appearing frills. Since some of the appeared frills have the same size as arterioles in the retinal image, we cannot select a structure element bigger than a certain limit, because in addition to the frills, some part of the data will be removed. Hence, we need another step to remove the remaining frills in the edge image.

3.3.2. CCA and applying adaptive filter locally on such components

This step is done to label the connected components in the resulting edge image. Since we have in mind 8 neighborhoods of pixels in the edge image, we consider a mask as in Figure 4. It is moved to the center of this mask on the pixels of the binary image if there is a pixel with a white color, p, to be labeled. If the labeled and unlabeled pixels are shown by * and –, respectively, we label the connected components in the image according to the following rules:

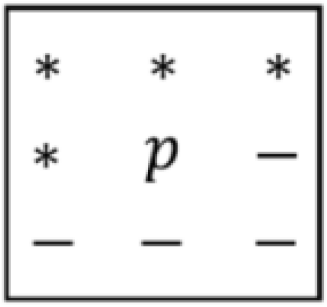

Figure 4. The 3 × 3 mask for the CCA.

- If all * have the label 0, we give a new label to the pixel p.
- If only one * has the label 1, we dedicate the label of that neighborhood to pixel p.
- If more than one * has the label 1, we give the label of one of the neighborhoods to pixel p and a sign to the labels as equivalence.

Now there is an image in which all of the connected blood vessels and arterioles have label 1. For local processing, the labeled image is divided into subimages and defines an adaptive threshold T [11] as:

$$T = \mu - \alpha\sigma, \tag{11}$$

where σ and μ are the adaptive values of above threshold and mean value and standard deviation of length of labels in each produced subimage, respectively. α is a constant value that controls the amount of the threshold T, where $\alpha < 1$ and is usually obtained by trial-and-error method.

The aforesaid filter acts so that it recognizes the labeled components whose lengths are lower than the threshold T as noise and removes them.

4. Results

4.1. Database

This approach was applied to the well-known database DRIVE [12]. From this database, 40 images were selected from the images related to 400 diabetic patients, ranging between 50 to 90 years of age, in the Netherlands. The images in this database are of 584 × 565 pixels and in JPEG format.

4.2. Evaluation parameters

To evaluate our algorithm for enhancing the contrast, we can use 2 criteria, the peak signal-to-noise ratio (PSNR) and the contrast increase index (CII). The equations for the PSNR and CII are defined as follows:

$$PSNR = 10\log_{10}\frac{Max_{I^2}}{MSE}, \quad MSE = \frac{1}{mn}\sum_{i=1}^{m}\sum_{j=1}^{n}\|I_o(i,j) - I_e(i,j)\|^2. \tag{12}$$

Here, MAX_I and MSE are the maximum illumination and mean squared error of the image, respectively. I_o is the original image and I_e is the enhanced image.

$$CII = \frac{C_{Enhanced}}{C_{Original}}, \quad C = \frac{r-b}{r+b} \tag{13}$$

Here, $C_{Enhanced}$ and $C_{Original}$ are the contrast of the enhanced and original images, respectively, and r and b are the mean values of the gray-level of the foreground and background of the image, respectively.

Considering the segmented images by humans in the DRIVE database, the following 2 criteria are defined in order to compare the results from the algorithm with the results from the segmentation by the specialist:

- True positive (TP): Indicates the pixels that the algorithm recognized as blood vessels, and, in fact, they are related to the blood vessels.
- False positive (FP): Indicates the pixels that the algorithm recognized as blood vessels, but, in fact, they are not related to the blood vessels.
- True negative (TN): Indicates the pixels that the algorithm did not recognize as blood vessels, and, in fact, they are not related to the blood vessels.
- False negative (FN): Indicates the pixels that the algorithm did not recognize as blood vessels, but, in fact, they are related to the blood vessels.

TPR is the ratio of true positives to all of the pixels belonging to the blood vessels, FPR is the ratio of false positives to all of the pixels that do not belong to the blood vessels, TNR is the ratio of true negatives to all of the pixels that do not belong to the blood vessels, and FNR is the ratio of false negatives to all of the pixels belonging to the blood vessels.

4.3. Preprocessing

It is noteworthy that different parameter values in the preprocessing and main processing stages are selected for implementation by the method of trial and error. For example, in the correction functions, the best possible values are selected according to the desired application.

This section deals with the results from applying some of the aforesaid steps in image 21 from the DRIVE database. In the selecting a proper subband section, we chose the criterion $C_{\mu r}$ as 0.45: that is, if $C_{\mu r} > 0.45$, the illumination of the subimage of band G is proper and we use only the subimage of band G; otherwise, we use histogram matching with the aid of subband R to increase the dynamic range of the gray level of subband G. In our algorithm, the adaptive function parameters a, p, k, k_1, k_2, and k_3 are set to a = 1, p = 0.1, k = 1, $k_1 = 1.1$, $k_2 = 1.4$, and $k_3 = 1$, heuristically.

We also estimate the standard deviation of the image by the mask and the following equation in the spatial domain [9]:

$$\sigma = \sqrt{\frac{\pi}{2}} \frac{1}{6(k-2)(l-2)} \sum |f(x,y) * M, |M = \begin{bmatrix} 1 & -2 & 1 \\ -2 & 4 & -2 \\ 1 & -2 & 1 \end{bmatrix}, \tag{14}$$

where f is the original image and $(k \times l)$ is the size of the image. In this paper, we use the 'wrapping' method to implement the fast discrete curvelet transform in the discrete domain. The wrapping implementation is simpler,

faster, and less redundant than the existing proposals. We use 5 bands, in which the images are analyzed with various scales, to apply the curvelet transform. Moreover, the angular accuracy is selected as 22.5° in the first scale; that is, 16 directions are selected in the first scale. Figures 5a and 5b show the results of the preprocessing stage. By applying the preprocessing algorithm, the mean value and standard deviation of all of the retinal images in the database are given in Table 1.

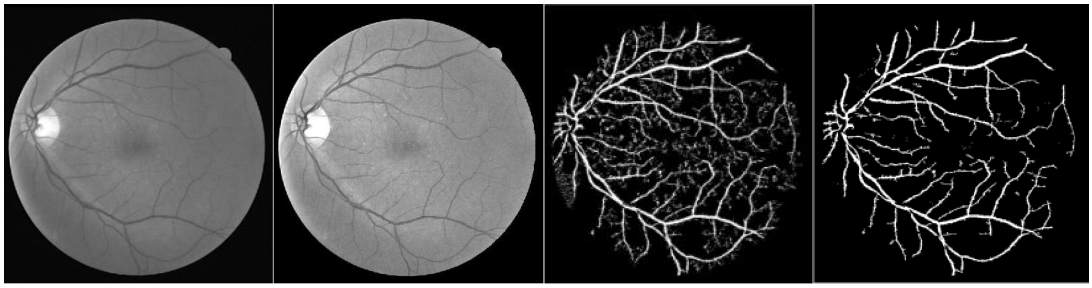

Figure 5. a) The best subband of original image; b) the enhanced image in terms of illumination and contrast, PSNR = 29.813, CII = 1.155; c) the extracted blood vessels with frills; and d) the final extracted blood vessels, TPR = 0.8612, FPR = 0.0157, accuracy = 0.9593.

Table 1. Image enhancement results for all retinal images on DRIVE database.

Quantitative criterion	Mean value	Standard deviation
PSNR	29.730	1.008
CII	1.146	0.019

Scientific papers define the proper values for the PSNR as 30 and above, indicating the noise being removed successfully. This value depends also on the studied image. As shown in Table 1, the proposed method reaches this value.

4.4. Extraction results

We determine the size of the multidirectional elements as 9 × 9 in order to not be sensitive to partial changes and to have the ability of extracting the arterioles as well. Thus, we determine the angular accuracy as 11.25°. Figures 5c and 5d show the extracted blood vessels with and without frills.

To remove the frills with the aid of the opening functor based on the geodesic conversions, we use a 5 × 5 simple square structuring element as the structure element. Considering 8 neighborhoods and the CCA, we label the connected components of the image. Next, after dividing the image into blocks of 90 × 90 pixels, we apply the adaptive filter with the aforesaid threshold for all of the blocks locally. The components whose lengths are lower than the threshold T are recognized as noise and removed. Figure 6 shows some final results of the blood vessel extraction in other images from the DRIVE database. The aforesaid assessment criteria in Section 3.2 and the mean accuracy of the algorithm are calculated for all of the existing images in the database. The results are given in Table 2. Table 2 shows the extraction results based on the TPR, FPR, and accuracy parameters. As shown, the blood vessels are extracted from background at a high accuracy of 96.15%.

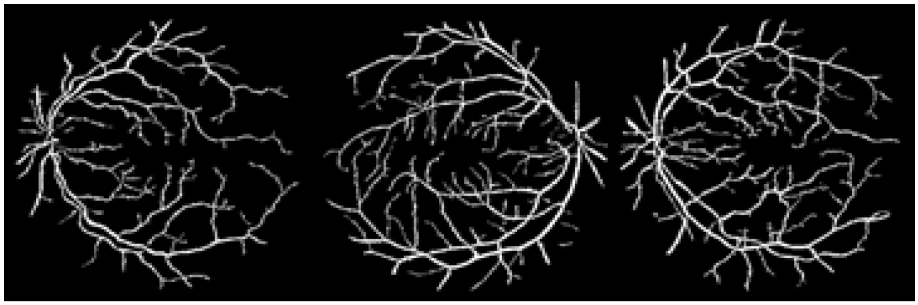

Figure 6. Extracted blood vessels from: a) image 9 with TPR = 0.8591, FPR = 0.0126, accuracy = 0.9585; b) image 13 with TPR = 0.8620, FPR = 0.0121, accuracy = 0.9603; c) image 35 with TPR = 0.8642, FPR = 0.0139, accuracy = 0.9612.

Table 2. Blood vessel extraction results for all images.

Algorithm	TPR	FPR	Average accuracy (%)
Our algorithm	0.8631	0.0164	96.15

4.5. Comparison with other algorithms

Table 3 compares the performance of the proposed algorithm and some earlier reported methods based on the DRIVE database in extracting the blood vessels from the retinal images. The algorithm proposed by Mendonça and Campilho [4] used mathematical morphology to benefit from a priori known vasculature shape features, such as being piecewise linear and connected. By applying morphological operators, the vasculature was then filtered from the background for the final segmentation. The assumption that vessels are elongated structures was the basis for the supervised ridge-based vessel detection method presented by Staal et al. [13]. Ridges were extracted from the image and used as primitives to form line elements. Each pixel was then assigned to its nearest line element, the image thus being partitioned into patches. For every pixel, 27 features were first computed and those obtaining the best class separability were finally selected. Feature vectors were classified using a k-nearest neighbor classifier and sequential forward feature selection. Martinez-Perez et al. [14] proposed a method based on multiscale feature extraction. The local maxima over the scales of the gradient magnitude and the maximum principal curvature of the Hessian tensor were used in a multiple pass region growing procedure. Growth progressively segmented the blood vessels, using both feature and spatial information. Marín et al. [15] presented a supervised method for blood vessel detection in digital retinal images. This method uses a neural network scheme for pixel classification and computes a 7-dimensional vector composed of gray level- and moment invariant-based features for pixel representation.

Table 3. Comparison of blood vessel extraction algorithms for retinal images.

Method	TPR	FPR	Average accuracy (%)	Database	Run time (s)
Mendonça and Campilho [4]	0.7344	0.0236	94.63	DRIVE	—
Staal et al. [13]	0.6780	0.0170	94.41	DRIVE	—
Martinez-Perez et al. [14]	0.7246	0.0345	93.44	DRIVE	—
Marín et al. [15]	0.7068	0.0305	94.52	DRIVE	—
Our algorithm	0.8631	0.0164	96.15	DRIVE	21

In our algorithm, applying the preprocessing techniques effectively omits the high intensity variations, and then the proposed morphology function introduced with multidirectional structure elements easily extracts the blood vessels from the retinal images. Finally, using the CCA analysis, the created noise in the edge images is effectively omitted.

Our experiments show that applying the curvelet transform in the preprocessing stage can increase the system's accuracy as well as stability in the accuracy of the algorithm.

5. Conclusion

Having considered the criteria for assessing the methods used for enhancing the contrast of the images and extracting the blood vessels, it can be concluded that the proposed algorithm is a success in fulfilling the goals.

Since the preprocessing phase plays an important role in the final extraction results, applying the BotHat morphology functor locally and histogram stretching on the retinal image will have a noticeable effect on both having the retinal images with uniform illumination as well as improving the accuracy of the final edge image.

Considering the aforesaid attributes of the curvelet transform, it is seen that, on one hand, this developed instrument serves successfully in enhancing the contrast of the images and, on the other hand, proper selection of the corrective function and proper setting of parameters resulted in preventing the strengthening of the noise while enhancing the contrast.

In the method of morphology with multidirectional structure elements, the structure elements act with more power in recognizing the edge. Of course, there are some frills in the edge image due to the changes in the illumination of the background. These frills are removed effectively by the geodesic conversion-based morphology functors, CCA and local implementation of the adaptive filter on these components. According to the definitions in Section 3.2, the accuracy of the algorithm is defined as shown below.

$$Acc = (TP + TN)/(TP + FN + TN + FP) \tag{15}$$

According to Table 2 and considering that the algorithm can extract the blood vessels from the retinal images with a high accuracy of 96.15% in good time, it can be used as a fast and reliable method.

Acknowledgment

The author would like to thank the authors of the DRIVE database for making their data publicly available. The author would also like to thank Dr. Forough Sadatian, Dr. Maedeh Motamedi and Dr. Parvaneh Shayeste for their technical advices.

References

[1] C. Wu, G. Agam, P. Stanchev, "A general framework for vessel segmentation in retinal images", Proceedings of the IEEE International Symposium on Computational Intelligence in Robotics and Automation, pp. 37–42, 2007.

[2] S. Supot, C. Thanapong, P. Chuchart, S. Manas, "Automatic segmentation of blood vessels in retinal image based on fuzzy k-median clustering", Proceedings of the IEEE International Conference on Integration Technology, pp. 584–588, 2007.

[3] K. Estabridis, R. Defigueiredo, "Blood vessel detection via a multiwindow parameter transform", Proceedings of the 19th IEEE Symposium on Computer-Based Medical Systems, pp. 424–429, 2006.

[4] A.M. Mendonça, A. Campilho, "Segmentation of retinal blood vessels by combining the detection of centerlines and morphological reconstruction", IEEE Transactions on Medical Imaging, Vol. 25, pp. 1200–1213, 2006.

[5] S. Shahbeig, H. Pourghassem, "Blood vessels extraction in retinal image using new generation curvelet transform and adaptive weighted morphology operators", Intelligent Systems in Electrical Engineering, Vol. 3, pp. 63-76, 2013.

[6] S. Shahbeig, H. Pourghassem, "Fast and automatic algorithm for optic disc extraction in retinal images using principle-component-analysis-based preprocessing and curvelet transform", Journal of the Optical Society Of America A-Optics Image Science and Vision, Vol. 30, pp. 13-21, 2013.

[7] P. Salembier, L. Torres, E. Masgrau, M.A. Lagunas, "Comparison of some morphological segmentation algorithms based on contrast enhancement application to automatic defect detection", Signal Processing V: Theories and Applications, Vol. 2, pp. 833–836, 1990.

[8] E.J. Candès, "Harmonic analysis of neural networks", Applied and Computational Harmonic Analysis, Vol. 6, pp. 197–218, 1999.

[9] Z.B. Zhao, J.S. Yuan, Q. Gao, Y.H. Kong, "Wavelet image de-noising method based on noise standard deviation estimation", Proceedings of the IEEE International Conference on Wavelet Analysis and Pattern Recognition, Vol. 4, pp. 1910–1914, 2007.

[10] R.C. Gonzalez, R.E. Woods, Digital Image Processing, Upper Saddle River, NJ, USA, Prentice Hall, 2002.

[11] S. Shahbeig, "Automatic and quick blood vessels extraction algorithm in retinal images", IET Image Processing, Vol. 7, pp. 392-400, 2013.

[12] Image Sciences Institute, DRIVE database, available at http://www.isi.uu.nl/Research/Databases/DRIVE/download.php.

[13] J. Staal, M.D. Abràmoff, M. Niemeijer, M.A. Viergever, B. Van Ginneken, "Ridge-based vessel segmentation in color images of the retina", IEEE Transactions on Medical Imaging, Vol. 23, pp. 501–509, 2004.

[14] M.E. Martinez-Perez, A.D. Hughes, S.A. Thom, A.A. Bharath, K.H. Parker, "Segmentation of blood vessels from red-free and fluorescein retinal images", Medical Image Analysis, Vol. 11, pp. 47–61, 2007.

[15] D. Marín, A. Aquino, M.E. Gegúndez-Arias, J.M. Bravo, "A new supervised method for blood vessel segmentation in retinal images by using gray-level and moment invariants-based features", IEEE Transactions on Medical Imaging, Vol. 30, pp. 146–158, 2011.